medRxiv preprint doi: https://doi.org/10.1101/19002782; this version posted July 22, 2019. The copyright holder for this preprint (which was not certified by peer review) is the author/funder, who has granted medRxiv a license to display the preprint in perpetuity.
All rights reserved. No reuse allowed without permission.

Mechanisms of Arrhythmogenicity in Hypertrophic Cardiomyopathy: Insight from Noninvasive Electrocardiographic Imaging

Erick A. Perez-Alday[1], PhD, Kazi T. Haq[1], PhD, David M. German[1], MD, Christopher Hamilton[1], BA, Kyle Johnson[1], BS, Francis Phan[1], MD, Nichole M. Rogovoy[1], BS, Katherine Yang[1,2], BS, Ashley Wirth[1], BS, Jason A.Thomas[1], BS, Khidir Dalouk[1,3], MD, Cristina Fuss[4], MD, Maros Ferencik[1], MD, PhD, MCR, Stephen Heitner[1] MD, Larisa G. Tereshchenko[1], MD, PhD.

[1]Knight Cardiovascular Institute, Oregon Health & Science University, Portland, OR; [2]Sidney Kimmel Medical College, Philadelphia, PA; [3] Portland VA Medical Center, Portland, OR; [4]Department of Diagnostic Radiology, Oregon Health & Science University, Portland, OR

Correspondence: Larisa Tereshchenko, 3181 SW Sam Jackson Park Rd; UHN62; Portland, OR, 97239. E-mail:tereshch@ohsu.edu. Phone:503-494-7400; Fax:503-494-8550.

Brief Title: ECGi insight into HCM mechanisms

Subject Codes: electrophysiology

Clinical Trial Registration−URL: www.clinicaltrials.gov Unique identifier: NCT02806479

Words: 6605

medRxiv preprint doi: https://doi.org/10.1101/19002782; this version posted July 22, 2019. The copyright holder for this preprint (which was not certified by peer review) is the author/funder, who has granted medRxiv a license to display the preprint in perpetuity.
All rights reserved. No reuse allowed without permission.

Abstract

Background—Mechanisms of arrhythmogenicity in hypertrophic cardiomyopathy (HCM) are not well understood. We hypothesized that HCM is characterized by the specific electrophysiological substrate as compared to patients with ischemic cardiomyopathy (ICM), or healthy individuals.

Methods—We conducted a prospective case-control study. HCM patients at high risk for ventricular tachyarrhythmia (VT) (n=10; age 61±9 y; left ventricular ejection fraction (LVEF) 60±9%) and three control groups (Healthy individuals (n=10; age 28±6 y; LVEF>70%), ICM patients with LV hypertrophy (LVH) and known VT (n=10; age 64±9 y; LVEF 31±15%), and ICM patients with LVH, and no known VT (n=10; age 70±7y; LVEF 46±16%). All participants underwent 12-lead ECG, cardiac CT or MRI, and 128-electrode body surface mapping (BioSemi ActiveTwo, Netherlands). Non-invasive voltage and activation maps were reconstructed using the open-source SCIRun (University of Utah) inverse problem-solving environment.

Results—In endocardial basal anterior segment, HCM patients had the slowest ventricular conduction [54.3±8.6 vs. 64.0±8.0 (ICM with VT) vs. 63.3±5.4 (ICM no VT) vs. 66.1±5.4 cm/s (Healthy); P=0.019], the largest unipolar voltage [1086±241 vs. 982±230 (ICM with VT) vs. 853±281 (ICM no VT) vs. 802±108 μV (Healthy); P=0.016], and the greatest voltage dispersion [median(interquartile range) 178(162-276) vs. 146(89-157) (ICM with VT) vs. 161(102-214) (ICM no VT) vs. 101(53-147) μV (Healthy); P=0.017]. Differences were also observed in other endo-and epicardial basal and apical segments.

Conclusion—Ventricular conduction velocity is slower in HCM when compared with ICM, even in myocardial segments remote from the region of maximal wall thickness, suggesting a distinct electrophysiological substrate in HCM.

medRxiv preprint doi: https://doi.org/10.1101/19002782; this version posted July 22, 2019. The copyright holder for this preprint (which was not certified by peer review) is the author/funder, who has granted medRxiv a license to display the preprint in perpetuity.
All rights reserved. No reuse allowed without permission.

Clinical Trial Registration−URL: www.clinicaltrials.gov Unique identifier: NCT02806479

Keywords—hypertrophic cardiomyopathy, electrocardiographic imaging, body surface mapping, conduction velocity.

medRxiv preprint doi: https://doi.org/10.1101/19002782; this version posted July 22, 2019. The copyright holder for this preprint (which was not certified by peer review) is the author/funder, who has granted medRxiv a license to display the preprint in perpetuity.
All rights reserved. No reuse allowed without permission.

Introduction

Patients with hypertrophic cardiomyopathy (HCM) are at high risk of life-threatening ventricular arrhythmias and sudden cardiac death (SCD).[1] Mechanisms of arrhythmogenicity in HCM are complex and incompletely understood. It was previously shown that the late sodium current is increased in HCM, suggesting the importance of repolarization abnormalities.[2] At the same time, cardiac magnetic resonance (CMR) studies have shown that the myocardium in HCM is characterized by increased fibrosis burden, supporting an alternative mechanism for arrhythmogenesis - heterogeneity in electrical activation. The degree of late gadolinium enhancement in HCM is associated with SCD and appropriate implantable cardioverter-defibrillator (ICD) therapy.[3] Previously, a similar frequency of both reentrant monomorphic ventricular tachycardia (VT) and ventricular fibrillation (VF) was observed in HCM patients with ICD,[4] suggesting similarity of mechanisms with ischemic cardiomyopathy (ICM). While the presence of patchy scar in HCM suggests likely similarity in macro-reentrant VT mechanisms with post-myocardial infarction (MI) VT, VT ablation in HCM is less successful than in post-infarction VT. In HCM patients who underwent VT ablation, the incidence of VT recurrence, death, and cardiac transplantation at one year was one of the highest amongst all non-ischemic cardiomyopathies (NICM),[5] even after adjusting for comorbidities. This may be due to anatomic limitations for ablation (predominantly mid-myocardial septal location of the scar), or diffuse nature of cardiomyocyte disarray and interstitial fibrosis that features histopathological hallmark of HCM[6]. By and large, electrophysiological (EP) substrate in HCM is incompletely understood. Recently, the non-invasive electrocardiographic imaging (ECGi), a state-of-the-art technology, became available as a tool to study mechanisms of cardiac arrhythmias.[7] We

medRxiv preprint doi: https://doi.org/10.1101/19002782; this version posted July 22, 2019. The copyright holder for this preprint (which was not certified by peer review) is the author/funder, who has granted medRxiv a license to display the preprint in perpetuity.
All rights reserved. No reuse allowed without permission.

designed this study with the goal to describe the EP substrate of HCM, in comparison to relatively well-understood EP substrate of post-infarction macro-reentrant VT.

Methods

Study population: inclusion and exclusion criteria

We conducted a single-center case-control study of high-risk HCM cases with three control groups (Clinical Trial Registration—URL: www.clinicaltrials.gov Unique identifier: NCT02806479). The study was approved by the Oregon Health & Science University (OHSU) Institutional Review Board (IRB), and all participants signed an informed consent form. Enrollment was performed at OHSU in 2016-2018. Adult (age≥18y) non-pregnant participants were enrolled if the inclusion and exclusion criteria were met, as described below.

Inclusion criteria for HCM group were: (1) history of resuscitated sudden cardiac arrest, or documented sustained VT, or (2) maximal left ventricular (LV) wall thickness above 30 mm, or extensive fibrosis on CMR (above 10% of total myocardial volume), or (3) high risk of SCD (>7.5%/5y) as determined by HCM risk-SCD[8] score.

Healthy control group I (*Healthy*) was designed to include individuals who were free from structural heart disease and arrhythmogenic substrate in ventricles. The inclusion criterion required evaluation by a cardiac electrophysiologist for AV nodal reentrant tachycardia. Exclusion criteria were diagnosed structural heart disease, or known risk factors of structural heart disease[9] (history of hypertension, smoking, diabetes, body mass index < 18.5 or >30 kg/m^2, and family history of coronary heart disease (CHD) diagnosed at age 50 or younger).

medRxiv preprint doi: https://doi.org/10.1101/19002782; this version posted July 22, 2019. The copyright holder for this preprint (which was not certified by peer review) is the author/funder, who has granted medRxiv a license to display the preprint in perpetuity.
All rights reserved. No reuse allowed without permission.

Control group II (*post-MI VT-free*) included post-MI patients without a history of sustained ventricular tachyarrhythmias, as shown either by the history of freedom from sustained VT/VF during at least one generator life of primary prevention ICD, or medical record.

Control group III (*post-MI VT*) included post-MI patients with arrhythmogenic substrate as proven by the history of sudden cardiac arrest and implanted secondary prevention ICD, or, if ICD was implanted for primary prevention of SCD, and there was documented sustained (cycle length < 240ms) VT/VF event treated by appropriate ICD shock. MADIT-RIT programming criteria were applied, to avoid inclusion of treated non-sustained VT events. Sudden cardiac arrest due to a transient cause was an exclusion criterion.

In addition, exclusion criteria for all study participants were the age of less than 18y, pregnancy, persistent atrial fibrillation (AF), chronic (above 5%) right ventricular (RV) or biventricular pacing, renal insufficiency with estimated glomerular filtration rate (eGFR) < 30 ml/min, congenital heart disease, and contraindications for CMR or cardiac computed tomography (CT) with contrast. By design, we planned to enroll 10 participants in each group.

Cardiac imaging and assessment of cardiac structure and function

Healthy controls underwent non-contrast CMR using a Siemens TIM Trio 3 Tesla with VB17 software and Siemens Prisma Fit 3 Tesla scanner with E11C software. The other three groups underwent prospectively ECG-triggered contrast-enhanced 256-detector row cardiac CT (Philips iCT, Philips Medical Imaging, Cleveland, OH). The images were acquired in mid to end diastole with a slice thickness of 0.6 mm and in-plane resolution of approximately 0.5 mm. All cardiac CT and CMR images were reviewed by a cardiologist (DMG) and ventricular volumes were obtained in a semiautomatic fashion using commercially available software (IntelliSpace Portal; Philips Healthcare, Redmond, WA, USA; and CVI42; Circle Cardiovascular Imaging Inc.,

medRxiv preprint doi: https://doi.org/10.1101/19002782; this version posted July 22, 2019. The copyright holder for this preprint (which was not certified by peer review) is the author/funder, who has granted medRxiv a license to display the preprint in perpetuity.
All rights reserved. No reuse allowed without permission.

Calgary, Alberta, Canada). The standardized myocardial segmentation and nomenclature[10] were used to define 17 segments of LV.

Additionally, data from the most recent echocardiogram was abstracted to provide additional information on baseline cardiac structure and function. For subjects who underwent CMR, left ventricular ejection fraction (LVEF) was calculated from ventricular volume measurements. For all other individuals, LVEF was calculated from the echocardiogram using the biplane Simpson method of discs. Regional LV function was evaluated by the echocardiographic wall motion score index. Motion and systolic thickening in each segment were scored as: normal or hyperkinesis = 1, hypokinesis = 2, akinesis = 3, and dyskinesis (or aneurysmal) = 4. Wall motion score index was calculated as the sum of all scores divided by the number of visualized segments. Resting peak LVOT gradient was calculated for all participants. In addition, HCM participants had peak LVOT gradient measured during Valsalva maneuver and at peak exertion.

Body surface potentials recording and ECG electrodes localization

A routine clinical resting 12-lead electrocardiogram (ECG) was recorded during the study visit, and ECG metrics were measured by the 12 SL algorithm (GE Marquette Electronics, Milwaukee, WI).

Unipolar ECG potentials were recorded on the body surface using the ActiveTwo biopotential measurement system (BioSemi, Amsterdam, the Netherlands) with 128 Ag/AgCL electrodes (4 panels of 32 electrodes; each panel is arranged as four strips of 8-electrodes; diameter of the ECG electrodes 5 mm), as previously described.[11] The sampling rate of the signal was 16,384 Hz; bandwidth DC-3,200 Hz. ECG electrodes were localized by three-dimensional (3D) photography approach, using a Kinect camera (Microsoft, Redmond, WA, USA), as

medRxiv preprint doi: https://doi.org/10.1101/19002782; this version posted July 22, 2019. The copyright holder for this preprint (which was not certified by peer review) is the author/funder, who has granted medRxiv a license to display the preprint in perpetuity.
All rights reserved. No reuse allowed without permission.

previously reported.[11] In addition, for co-registration of torso images, five CMR- or CT- specific markers were placed on each patient's chest during scanning, to mark ECG electrodes locations.

Reconstruction of torso and heart meshes

We constructed 3D meshes of a continuous surface of the endocardium (excluding papillary muscles) and epicardium of both ventricular chambers. The 3D heart and torso meshes were reconstructed using a semi-automatic approach – image growing method of a continuous surface[11, 12] from CMR/CT images using ITK-snap software (PICSL, USA).[13] Each cardiac mesh was manually reviewed to ensure a continuous segmentation of epicardium and endocardium of both ventricular chambers and exclude atria chambers and papillary muscles. Both torsi meshes segmented by the 3D photography method, and DICOM images were matched using the co-registered CMR/CT markers and electrode position, as previously described.[11] The resolution of the cardiac mesh was 3.6 ± 0.5 mm with 3992 ± 735 nodes.

Inverse solution and reconstruction of the cardiac activation map

The workflow is shown in Figure 1. One clean normal sinus beat was selected for analysis; an absence of extrasystole before and after selected beat was verified. We used the open-source SCIRun problem-solving environment developed at the Center for Integrative Biomedical Computing (University of Utah, UT),[14, 15] which was previously used to compute forward and inverse solutions[16] and reconstruct unipolar epicardial and endocardial electrograms (EGMs). The inverse problem was solved as the potential-based formulation (boundary element method), as a weighted minimum norm problem by applying a Tikhonov L2-norm regularization.

The steepest downslope of each unipolar EGM was determined automatically, using MATLAB (The MathWorks Inc, Natick, MA) software application. Then, each pair of neighboring unipolar EGMs together with resulting bipolar EGM (calculated as their difference)

medRxiv preprint doi: https://doi.org/10.1101/19002782; this version posted July 22, 2019. The copyright holder for this preprint (which was not certified by peer review) is the author/funder, who has granted medRxiv a license to display the preprint in perpetuity.
All rights reserved. No reuse allowed without permission.

was reviewed by at least two investigators (AW, KY, NMR, EAPA) blinded to the study groups assignment, to verify the consistency of morphology and the steepest downslope detection (Figure 2). Unipolar EGMs were excluded from further analysis in case of disagreement between all 3 EGMs. Recalculation of the steepest downslope was performed in case of morphology agreement but steepest downslope disagreement detection. For calculation of the time reference point, the three limb leads (I, II, and III) were used to define the averaged QRS onset on the surface ECG. Local activation time (LAT) in each node of the mesh was calculated as the time difference between averaged (surface ECG) QRS onset and the time of the steepest downslope on a corresponding unipolar EGM. To reconstruct cardiac activation map on the epicardial and endocardial surface, LAT was plotted in each epicardial and endocardial node.

Unipolar voltage potential map

Unipolar voltage was measured in each reconstructed EGM, and a unipolar voltage potential maps were constructed. The peak-to-peak voltage on each unipolar EGM was automatically measured using MATLAB (The MathWorks Inc, Natick, MA) software application. An accuracy of unipolar EGM peaks detection was validated by investigators (AW, KY, NMR, EAPA) blinded to groups assignment. We used the standardized myocardial segmentation and nomenclature[10] to define 17 segments of LV. Mean unipolar voltage was calculated for each segment. RV endocardial surface in 5 segments (basal anteroseptal and inferoseptal, mid-cavity anteroseptal and inferoseptal, and apical septal) served as an “epicardial” surface of LV. Standard deviation (SD) of unipolar voltage distribution in each segment served as a measure of voltage dispersion within each segment.

medRxiv preprint doi: https://doi.org/10.1101/19002782; this version posted July 22, 2019. The copyright holder for this preprint (which was not certified by peer review) is the author/funder, who has granted medRxiv a license to display the preprint in perpetuity.
All rights reserved. No reuse allowed without permission.

Ventricular Conduction Velocity

Ventricular conduction velocity between each pair of neighboring nodes was calculated as a distance between nodes divided by the difference in LATs between corresponding nodes. Mean conduction velocity was calculated for each LV segment.[10] RV endocardial surface in 5 segments (basal anteroseptal and inferoseptal, mid-cavity anteroseptal and inferoseptal, and apical septal) served as an "epicardial" surface of LV. Dispersion of conduction velocity was measured as SD of ventricular conduction velocity in each segment.

Statistical analysis

Statistics of normally distributed variables are summarized as mean ± SD. Distributions of all variables were reviewed. Outliers of ventricular conduction velocity representing non-physiological values (> 100cm/s) were removed from further analyses. After verifying the normality of distribution, we tested the hypothesis that the means (mean voltage and mean conduction velocity) are the same across four study groups while removing the assumption of equal covariance matrices. The Wald chi-squared statistic with James's approximation[17] was used to calculate P-values.

We used a Kruskal–Wallis test of the hypothesis that four study groups are from the same population, to compare voltage and velocity dispersions (measured as an SD of velocity and voltage in each of 17 segments[10]), which have a non-normal distribution. Non normally distributed variables are summarized as the median and interquartile range (IQR).

A P-value of less than 0.05 was considered significant. Statistical analyses were performed using STATA MP 15.1 (StataCorp LLC, College Station, TX).

medRxiv preprint doi: https://doi.org/10.1101/19002782; this version posted July 22, 2019. The copyright holder for this preprint (which was not certified by peer review) is the author/funder, who has granted medRxiv a license to display the preprint in perpetuity.
All rights reserved. No reuse allowed without permission.

Results

Study population

Clinical characteristics of the study population are shown in Table 1. Most of HCM patients (80%) had previously undergone genetic testing. The definitive, disease-causing *MYHBPC3* mutation was found in 2 patients. Half of the HCM participants had survived a sudden cardiac arrest, and another half had documented the history of sustained VT/VF. While half of the HCM patients had a history of severe LVOT obstruction (up to 153 mmHg at peak exertion), they had already undergone surgical myectomy, resulting in vastly improved LVOT gradients (provoked peak LVOT gradient 20±20 mmHg), at the time of enrollment.

In VT-free post-MI group, the scar was located in the anteroseptal region in 90% of participants. In post-MI VT group, the scar was located in the inferoposterior region in 40% and anteroseptal in 60%. Single-chamber ICD was implanted in approximately 50% of groups II-III controls, and HCM. The other half of the population had a dual-chamber ICD implanted.

LV systolic function was normal in healthy controls and HCM participants, whereas ischemic cardiomyopathy (ICM) with reduced LVEF was confirmed for both post-MI groups (Table 1).

Mean unipolar voltage and unipolar voltage dispersion

A representative example of a voltage map is shown in Figure 3A. Mean unipolar voltage (Supplemental Table 1 and Figure 4) was significantly different across all 4 study groups in basal anteroseptal and apical septal segments, on both sides of septum – LV and RV endocardium. Also, a significant difference in voltage across all four groups was observed on both endocardial and epicardial surface of basal anterior and anterolateral segments, the endocardial surface of anterior apical segment, and the epicardial surface of basal inferior and mid-inferolateral

medRxiv preprint doi: https://doi.org/10.1101/19002782; this version posted July 22, 2019. The copyright holder for this preprint (which was not certified by peer review) is the author/funder, who has granted medRxiv a license to display the preprint in perpetuity.
All rights reserved. No reuse allowed without permission.

segments. Healthy individuals had the smallest mean unipolar voltage, whereas HCM was characterized by the largest voltage (Figure 4). Unipolar voltage in two post-MI groups was similar, and had intermediate values, as compared to healthy and HCM participants.

Voltage dispersion was significantly smaller in healthy controls, as compared to the other three groups (Supplemental Table 2 and Figure 5). Remarkably, in several segments, voltage dispersion in HCM was the highest amongst all four groups, significantly exceeding voltage dispersion in both ICM groups. The unipolar voltage dispersion was significantly different across study groups in both endocardial and epicardial segments in basal anterior, basal anterolateral and inferolateral, apical inferior, and the epicardial surface of the apex.

Mean ventricular conduction velocity and velocity dispersion

A representative example of the activation map is shown in Figure 3B. In Healthy controls, we observed a normal activation pattern, which initiated in the septal region and propagated from endocardium to epicardium, with several breakthroughs – near the RV apex and anterior paraseptal aspects of the epicardium in regions adjacent to the left anterior descendent coronary artery. Activation proceeded from apex to the inferior basal area in both RV and LV, with the inferolateral LV base and the region near right ventricular outflow tract (RVOT) being the latest to activate.

Overall, mean conduction velocity was mostly similar in all 4 study groups (Supplemental Table 4 and Figure 6). In most LV segments, there was no difference in mean conduction velocity in healthy as compared to both ICM groups. Mean conduction velocity was significantly slower in HCM participants as compared to other groups in endocardial basal anterior, and epicardial basal inferior, basal anterolateral, apical anterior, and apical septal segments.

medRxiv preprint doi: https://doi.org/10.1101/19002782; this version posted July 22, 2019. The copyright holder for this preprint (which was not certified by peer review) is the author/funder, who has granted medRxiv a license to display the preprint in perpetuity.
All rights reserved. No reuse allowed without permission.

Overall, velocity dispersion was largely similar across all four study groups. Velocity dispersion in HCM participants was significantly greater than in the other three groups only in one segment: RV endocardial surface corresponding to the basal anteroseptal segment (Supplemental Table 4).

Discussion

Our study revealed important features of EP substrate in HCM, which differentiate HCM substrate from ICM substrate in patients with VT history and post-MI scar located in the same areas (anterior and anteroseptal segments). HCM is characterized by significantly slower mean ventricular conduction velocity in many basal and apical segments, as compared to ICM. Areas of relatively slow ventricular conduction in HCM are large, and overall ventricular conduction slowing in HCM being diffuse. At the same time, the degree of ventricular conduction slowing was small, and mean ventricular conduction velocity remained within a range of normal values in all groups. Slow ventricular conduction facilitates the development and maintenance of reentrant VT. Diffuse nature of EP substrate in HCM may explain the low success rate of VT ablation in HCM, providing suggestions regarding the likelihood for success of VT ablation as a standing-alone long-term treatment solution for HCM. In the near future, the HCM registry study[18] may add understanding to the underlying cellular architecture of the myocardium and the impact of diffuse EP substrate in HCM.

EP substrate and mechanisms of arrhythmogenesis in HCM

HCM is the most common monogenic cardiac disease, with the incidence of up to 1 in 200 live births.[19] Diagnosis of HCM is challenging, although some preliminary machine learning studies are promising.[20, 21] Previous studies provided inconsistent results about the correlation between electroanatomical mapping with 3D-imaging in HCM. Aryana et al[22] reported a good

medRxiv preprint doi: https://doi.org/10.1101/19002782; this version posted July 22, 2019. The copyright holder for this preprint (which was not certified by peer review) is the author/funder, who has granted medRxiv a license to display the preprint in perpetuity.
All rights reserved. No reuse allowed without permission.

correlation between low voltage areas on the map, co-localized with a post-infarction scar in post-MI patients. However, scattered intramural fibrosis in HCM did not manifest by the low voltage on endocardial, nor epicardial maps. Reported findings included local conduction delay or conduction block, fractionated electrograms, and reduced voltage.[23] Hutchinson et al[24] showed that unipolar endocardial voltage mapping could accurately identify epicardial scar that is manifested by reduced unipolar voltage. Schumacher et al[23] also reported reduced bipolar voltage in the septal region in HCM patients.

In contrast, we observed significantly larger unipolar voltage in HCM as compared to healthy persons or ICM patients, and the difference was especially prominent in HCM-affected regions of the heart: both endocardial and epicardial basal and apical septal segments. The different methodology of voltage mapping may explain the observed discrepancy between our results and previous contact mapping studies. Our study is the first to report endocardial and epicardial voltage in HCM obtained by inverse solutions. A previous HCM case report[25] describing ECGi findings did not provide results of voltage map in its HCM patient. Consistently with our findings, Yoshida et al[26] in 1986 conducted body surface isopotential mapping and showed that HCM patients have significantly larger peak-to-peak voltage than patients with LVH due to essential hypertension.

We showed a greater degree of voltage dispersion in HCM as compared to post-MI patients in both endocardial and the epicardial segments in basal anterior, basal anterolateral and inferolateral, apical inferior, and the epicardial surface of the apex. This finding may be explained by an underlying phenomenon of diffused interstitial fibrosis in HCM, generating greater voltage dispersion as compared to patchy post-MI fibrosis. Further MRI studies[18] utilizing late gadolinium enhancement and T1-mapping are needed to evaluate the agreement

medRxiv preprint doi: https://doi.org/10.1101/19002782; this version posted July 22, 2019. The copyright holder for this preprint (which was not certified by peer review) is the author/funder, who has granted medRxiv a license to display the preprint in perpetuity.
All rights reserved. No reuse allowed without permission.

between voltage dispersion on ECGi voltage map and imaging-defined type of fibrosis, and their associations with clinical outcomes in HCM patients. HCM is characterized by a disorganized sarcomeric alignment, which can augment nonuniform anisotropic conduction, creating a substrate for reentry (both slow conduction and unidirectional block).[27] Disorganized bundles of ventricular fibers can lead to asymmetry in conduction. An impulse conducting in one direction meets a different sequence of muscle branching and changes in muscle bundle diameter, as compared to an impulse conducting in the opposite direction. Such asymmetry affects the source-sink relationships.[28]

Our findings are consistent with previous clinical observations in HCM, indicating that neither myectomy nor alcohol septal ablation reduces risk of SCD or VT. Most of HCM patients who undergo myectomy, develop left bundle branch block, and approximately a quarter of HCM patients who underwent alcohol septal ablation develop complete heart block.[29] Few case reports showed that a scar formed after alcohol septal ablation could serve as a substrate for reentrant VT[30]. Thus, surgical HCM treatment may reduce heart failure symptoms but do not change SCD risk in HCM. Diffuse nature of ventricular conduction slowing in HCM explains these previous clinical observations. Regardless of the type of intervention targeting reduction of septal thickness, diffused conduction slowing maintains pro-arrhythmic substrate facilitating the development of life-threatening reentrant VT.

Noninvasive mapping of ventricular activation

In this study, we used the Forward/Inverse problem toolkit from the SCIRun problem-solving environment, which is used by many investigators in the field.[14, 15, 31, 32] However, knowing the limitations of ECGi method,[33] we intentionally limited our analysis by averaged "per segment" data. Duchateau et al[33] observed mean activation time error of approximately 20 ms. In this

medRxiv preprint doi: https://doi.org/10.1101/19002782; this version posted July 22, 2019. The copyright holder for this preprint (which was not certified by peer review) is the author/funder, who has granted medRxiv a license to display the preprint in perpetuity.
All rights reserved. No reuse allowed without permission.

study, we observed ventricular activation dispersion of approximately 20 cm/s in all study participants, including healthy controls, with no meaningful differences in ventricular activation dispersion between groups. Therefore, we interpret that ventricular activation dispersion in our study quantifies an error of local ventricular conduction velocity measurement between two nods. Thus, we accept that actual ventricular conduction velocity can be on average either higher or lower by 20 cm/s. This study error precludes interpretations of specific ventricular conduction phenomena, yet our findings still provide insight into HCM mechanisms.

Limitations

A case-control study is susceptible to bias. We selected only high-risk HCM patients, and our HCM cases sample may not be representative of all HCM patients. To minimize selection bias, all control groups were enrolled in the same single center. Further development of inverse solution noninvasive activation mapping method is needed to enable interpretation of local ventricular activation patterns.

Acknowledgments:

The authors thank the study participants and staff. We thank William Woodward, ARMRIT, for the help with the CMR data acquisition.

Funding Sources:

The study was funded by Gilead Sciences, Inc, as a physician-initiated study. This work was partially supported by 1R01HL118277 and 2R56HL118277 (LGT).

Disclosures

The study was funded by Gilead Sciences, Inc, as physician-initiated study (LGT).

medRxiv preprint doi: https://doi.org/10.1101/19002782; this version posted July 22, 2019. The copyright holder for this preprint (which was not certified by peer review) is the author/funder, who has granted medRxiv a license to display the preprint in perpetuity.
All rights reserved. No reuse allowed without permission.

References

1. Maron MS, Rowin EJ, Wessler BS, Mooney PJ, Fatima A, Patel P, Koethe BC, Romashko M, Link MS and Maron BJ. Enhanced American College of Cardiology/American Heart Association Strategy for Prevention of Sudden Cardiac Death in High-Risk Patients With Hypertrophic Cardiomyopathy. *JAMA Cardiol*. 2019.

2. Coppini R, Ferrantini C, Yao L, Fan P, Del Lungo M, Stillitano F, Sartiani L, Tosi B, Suffredini S, Tesi C, Yacoub M, Olivotto I, Belardinelli L, Poggesi C, Cerbai E and Mugelli A. Late sodium current inhibition reverses electromechanical dysfunction in human hypertrophic cardiomyopathy. *Circulation*. 2013;127:575-84.

3. Mentias A, Raeisi-Giglou P, Smedira NG, Feng K, Sato K, Wazni O, Kanj M, Flamm SD, Thamilarasan M, Popovic ZB, Lever HM and Desai MY. Late Gadolinium Enhancement in Patients With Hypertrophic Cardiomyopathy and Preserved Systolic Function. *J Am Coll Cardiol*. 2018;72:857-870.

4. Cha YM, Gersh BJ, Maron BJ, Boriani G, Spirito P, Hodge DO, Weivoda PL, Trusty JM, Friedman PA, Hammill SC, Rea RF and Shen WK. Electrophysiologic manifestations of ventricular tachyarrhythmias provoking appropriate defibrillator interventions in high-risk patients with hypertrophic cardiomyopathy. *J Cardiovasc Electrophysiol*. 2007;18:483-7.

5. Vaseghi M, Hu TY, Tung R, Vergara P, Frankel DS, Di Biase L, Tedrow UB, Gornbein JA, Yu R, Mathuria N, Nakahara S, Tzou WS, Sauer WH, Burkhardt JD, Tholakanahalli VN, Dickfeld T-M, Weiss JP, Bunch TJ, Reddy M, Callans DJ, Lakkireddy DR, Natale A, Marchlinski FE, Stevenson WG, Della Bella P and Shivkumar K. Outcomes of Catheter Ablation of Ventricular Tachycardia Based on Etiology in Nonischemic Heart Disease: An International

medRxiv preprint doi: https://doi.org/10.1101/19002782; this version posted July 22, 2019. The copyright holder for this preprint (which was not certified by peer review) is the author/funder, who has granted medRxiv a license to display the preprint in perpetuity.
All rights reserved. No reuse allowed without permission.

Ventricular Tachycardia Ablation Center Collaborative Study. *JACC: Clinical Electrophysiology*. 2018;4:1141-1150.

6. Iles L, Pfluger H, Phrommintikul A, Cherayath J, Aksit P, Gupta SN, Kaye DM and Taylor AJ. Evaluation of diffuse myocardial fibrosis in heart failure with cardiac magnetic resonance contrast-enhanced T1 mapping. *J AmCollCardiol*. 2008;52:1574-1580.

7. Ramanathan C, Ghanem RN, Jia P, Ryu K and Rudy Y. Noninvasive electrocardiographic imaging for cardiac electrophysiology and arrhythmia. *NatMed*. 2004;10:422-428.

8. O'Mahony C, Jichi F, Pavlou M, Monserrat L, Anastasakis A, Rapezzi C, Biagini E, Gimeno JR, Limongelli G, McKenna WJ, Omar RZ, Elliott PM and Hypertrophic Cardiomyopathy Outcomes I. A novel clinical risk prediction model for sudden cardiac death in hypertrophic cardiomyopathy (HCM risk-SCD). *Eur Heart J*. 2014;35:2010-20.

9. Panel NE. Third Report of the National Cholesterol Education Program (NCEP) expert panel on detection, evaluation, and treatment of high blood cholesterol in adults (Adult Treatment Panel III). Final report. *Circulation*. 2002;106:278.

10. Cerqueira MD, Weissman NJ, Dilsizian V, Jacobs AK, Kaul S, Laskey WK, Pennell DJ, Rumberger JA, Ryan T and Verani MS. Standardized Myocardial Segmentation and Nomenclature for Tomographic Imaging of the Heart: A Statement for Healthcare Professional From the Cardiac Imaging Committee of the Council on Clinical Cardiology of the American Heart Association. *Circulation*. 2002;105:539-542.

11. Perez-Alday EA, Thomas JA, Kabir M, Sedaghat G, Rogovoy N, van Dam E, van Dam P, Woodward W, Fuss C, Ferencik M and Tereshchenko LG. Torso geometry reconstruction and

medRxiv preprint doi: https://doi.org/10.1101/19002782; this version posted July 22, 2019. The copyright holder for this preprint (which was not certified by peer review) is the author/funder, who has granted medRxiv a license to display the preprint in perpetuity.
All rights reserved. No reuse allowed without permission.

body surface electrode localization using three-dimensional photography. *J Electrocardiol*. 2018;51:60-67.

12. Alday EA, Colman MA, Langley P, Butters TD, Higham J, Workman AJ, Hancox JC and Zhang H. A new algorithm to diagnose atrial ectopic origin from multi lead ECG systems--insights from 3D virtual human atria and torso. *PLoS Comput Biol*. 2015;11:e1004026.

13. Yushkevich PA, Piven J, Hazlett HC, Smith RG, Ho S, Gee JC and Gerig G. User-guided 3D active contour segmentation of anatomical structures: significantly improved efficiency and reliability. *Neuroimage*. 2006;31:1116-1128.

14. Burton BM, Tate JD, Erem B, Swenson DJ, Wang DF, Steffen M, Brooks DH, van Dam PM and Macleod RS. A toolkit for forward/inverse problems in electrocardiography within the SCIRun problem solving environment. *Conf Proc IEEE Eng Med Biol Soc*. 2011;2011:267-70.

15. Coll-Font J, Burton BM, Tate JD, Erem B, Swenson DJ, Wang D, Brooks DH, van Dam P and Macleod RS. New Additions to the Toolkit for Forward/Inverse Problems in Electrocardiography within the SCIRun Problem Solving Environment. *Computing in cardiology*. 2014;2014:213-216.

16. Babaeizadeh S, Brooks DH, Isaacson D and Newell JC. Electrode boundary conditions and experimental validation for BEM-based EIT forward and inverse solutions. *IEEE transactions on medical imaging*. 2006;25:1180-8.

17. James G. Tests of linear hypotheses in univariate and multivariate analysis when the ratios of the population variances are unknown. *Biometrika*. 1954;41:19-43.

18. Kramer CM, Appelbaum E, Desai MY, Desvigne-Nickens P, DiMarco JP, Friedrich MG, Geller N, Heckler S, Ho CY, Jerosch-Herold M, Ivey EA, Keleti J, Kim DY, Kolm P, Kwong RY, Maron MS, Schulz-Menger J, Piechnik S, Watkins H, Weintraub WS, Wu P and Neubauer

medRxiv preprint doi: https://doi.org/10.1101/19002782; this version posted July 22, 2019. The copyright holder for this preprint (which was not certified by peer review) is the author/funder, who has granted medRxiv a license to display the preprint in perpetuity.
All rights reserved. No reuse allowed without permission.

S. Hypertrophic Cardiomyopathy Registry: The rationale and design of an international, observational study of hypertrophic cardiomyopathy. *Am Heart J*. 2015;170:223-30.

19. Semsarian C, Ingles J, Maron MS and Maron BJ. New perspectives on the prevalence of hypertrophic cardiomyopathy. *J Am Coll Cardiol*. 2015;65:1249-1254.

20. Rahman QA, Tereshchenko LG, Kongkatong M, Abraham T, Abraham MR and Shatkay H. Utilizing ECG-Based Heartbeat Classification for Hypertrophic Cardiomyopathy Identification. *IEEE Trans Nanobioscience*. 2015;14:505-12.

21. Green EM, van Mourik R, Wolfus C, Heitner SB, Dur O and Semigran MJ. Machine learning detection of obstructive hypertrophic cardiomyopathy using a wearable biosensor. *npj Digital Medicine*. 2019;2:57.

22. Aryana A, d'Avila A, Heist EK, Mela T, Singh JP, Ruskin JN and Reddy VY. Remote magnetic navigation to guide endocardial and epicardial catheter mapping of scar-related ventricular tachycardia. *Circulation*. 2007;115:1191-1200.

23. Schumacher B, Gietzen FH, Neuser H, Schummelfeder J, Schneider M, Kerber S, Schimpf R, Wolpert C and Borggrefe M. Electrophysiological characteristics of septal hypertrophy in patients with hypertrophic obstructive cardiomyopathy and moderate to severe symptoms. *Circulation*. 2005;112:2096-101.

24. Hutchinson MD, Gerstenfeld EP, Desjardins B, Bala R, Riley MP, Garcia FC, Dixit S, Lin D, Tzou WS, Cooper JM, Verdino RJ, Callans DJ and Marchlinski FE. Endocardial unipolar voltage mapping to detect epicardial ventricular tachycardia substrate in patients with nonischemic left ventricular cardiomyopathy. *Circ Arrhythm Electrophysiol*. 2011;4:49-55.

medRxiv preprint doi: https://doi.org/10.1101/19002782; this version posted July 22, 2019. The copyright holder for this preprint (which was not certified by peer review) is the author/funder, who has granted medRxiv a license to display the preprint in perpetuity.
All rights reserved. No reuse allowed without permission.

25. Ghosh S, Avari JN, Rhee EK, Woodard PK and Rudy Y. Hypertrophic cardiomyopathy with preexcitation: insights from noninvasive electrocardiographic imaging (ECGI) and catheter mapping. *J CardiovascElectrophysiol*. 2008;19:1215-1217.

26. Yoshida H, Imataki K, Nagahana H, Ihoriya F, Nakao Y, Saito D and Haraoka S. Cardiac hypertrophy in hypertrophic cardiomyopathy and hypertension evaluated by echocardiography and body surface isopotential mapping. *J Cardiogr*. 1986;16:399-406.

27. Spach MS and Josephson ME. Initiating reentry: the role of nonuniform anisotropy in small circuits. *J Cardiovasc Electrophysiol*. 1994;5:182-209.

28. Spach MS, Miller WT, III, Geselowitz DB, Barr RC, Kootsey JM and Johnson EA. The discontinuous nature of propagation in normal canine cardiac muscle. Evidence for recurrent discontinuities of intracellular resistance that affect the membrane currents. *CircRes*. 1981;48:39-54.

29. Khouzam RN and Naidu SS. Current status and future perspectives on alcohol septal ablation for hypertrophic obstructive cardiomyopathy. *Curr Cardiol Rep*. 2014;16:478.

30. Murata H, Miyauchi Y, Nitta T and Mizuno K. Electroanatomical mapping-guided endocardial and epicardial ablation of sustained ventricular tachycardia originating from alcohol septal ablation-induced scar in a patient with hypertrophic obstructive cardiomyopathy. *J Cardiovasc Electrophysiol*. 2010;21:1296-9.

31. Wang L, Gharbia OA, Nazarian S, Horacek BM and Sapp JL. Non-invasive epicardial and endocardial electrocardiographic imaging for scar-related ventricular tachycardia. *Europace*. 2018;20:f263-f272.

32. Cluitmans M, Brooks DH, MacLeod R, Dossel O, Guillem MS, van Dam PM, Svehlikova J, He B, Sapp J, Wang L and Bear L. Validation and Opportunities of

medRxiv preprint doi: https://doi.org/10.1101/19002782; this version posted July 22, 2019. The copyright holder for this preprint (which was not certified by peer review) is the author/funder, who has granted medRxiv a license to display the preprint in perpetuity.
All rights reserved. No reuse allowed without permission.

Electrocardiographic Imaging: From Technical Achievements to Clinical Applications. *Front Physiol*. 2018;9:1305.

33. Duchateau J, Sacher F, Pambrun T, Derval N, Chamorro-Servent J, Denis A, Ploux S, Hocini M, Jais P, Bernus O, Haissaguerre M and Dubois R. Performance and limitations of noninvasive cardiac activation mapping. *Heart Rhythm*. 2019;16:435-442.

medRxiv preprint doi: https://doi.org/10.1101/19002782; this version posted July 22, 2019. The copyright holder for this preprint (which was not certified by peer review) is the author/funder, who has granted medRxiv a license to display the preprint in perpetuity.
All rights reserved. No reuse allowed without permission.

Figure legends

Figure 1. Data analysis workflow from body surface potentials recordings to a reconstruction of ventricular activation map.

Figure 2. Quality control of measurement of the steepest downslope of epicardial electrogram (the steepest negative dV/dt, dashed line). Two neighboring unipolar electrograms (two upper rows) and bipolar electrogram (bottom row) are shown. Local activation time is marked by the dashed line.

Figure 3. Representative examples of (A) unipolar voltage and (B) ventricular activation maps in a healthy participant, during sinus rhythm activation. Superior, anterolateral, and posterior view. The orifices of the aorta and the mitral valve are combined.

Figure 4. Comparison of mean unipolar voltage in study groups, in 16 LV endocardial and 17 LV epicardial segments. Nomenclature: 1=basal anterior; 2=basal anteroseptal; 3=Basal inferoseptal; 4=Basal inferior; 5=Basal inferolateral; 6=Basal anterolateral; 7=Mid-anterior; 8=Mid-anteroseptal; 9=Mid-inferoseptal; 10=Mid-inferior; 11=Mid-inferolateral; 12=Mid-anterolateral; 13=Apical anterior; 14=Apical septal; 15=Apical Inferior; 16=Apical lateral; 17=apex. RV endocardial surface in 5 segments (basal anteroseptal and inferoseptal, mid-cavity anteroseptal and inferoseptal, and apical septal) served as an “epicardial” surface of LV.

Figure 5. Comparison of unipolar voltage dispersion in study groups, in 16 LV endocardial and 17 LV epicardial segments. Segments nomenclature as described in Figure 5 legend.

Figure 6. Comparison of mean ventricular conduction velocity in study participants, in 16 LV endocardial and 17 LV epicardial segments. Segments nomenclature as described in Figure 5 legend.

Table 1. Demographic and clinical characteristics of the study population

Characteristic	Healthy (n=10)	Post-MI VT-free (n=10)	Post-MI VT (n=10)	HCM (n=10)
Age(SD), y	28.8(5.6)	69.3(9.3)	64.0(10.5)	61.3(9.3)
Male, n(%)	4(40)	10(100)	10(100)	8(80)
White, n(%)	6(60)	10(100)	9(90)	10(100)
BMI(SD), kg/m^2	23.6(3.6)	33.0(6.6)	30.9(6.9)	30.1(5.7)
LVEF(SD), %	65.8(4.7)	45.8(15.4)	37.3(12.7)	60.4(8.3)
GLS(SD), %	-	-13.5(0)	-9.6(0.4)	-13.2(0.8)
LVIDd(SD), cm	4.3(0.4)	5.2(1.3)	6.1(1.1)	4.5(0.7)
LVIDs(SD), cm	2.7(0.4)	4.2(0.9)	5.1(1.4)	2.9(0.4)
LAVI(SD), ml/m^2	22.3(3.1)	32.6(13.9)	33.2(8.8)	40.1(12.8)
LVEDVI(SD), ml/m^2	76.7(13.4)	89.6(30.,0)	100.6(34.1)	72.2(12.3)
RVEDVI(SD), ml/m^2	89.0(20.5)	71.8(14.4)	76.7(10.8)	76.3(13.4)
LV mass index(SD),g/m^2	63.9(13.9)	76.0(15.0)	92.2(25.7)	99.3(28.9)
IVSd(SD), cm	0.8(0.1)	1.5(1.4)	1.0(0.1)	1.5(0.3)
LVPWd(SD), cm	0.8(0.1)	1.1(0.2)	1.0(0.2)	1.2(0.3)
E/A ratio	1.7(0.2)	1.3(0.8)	0.9(0.2)	1.0(0.4)
E/e’ ratio	5.9(1.5)	9.1(3.4)	11.4(5.7)	9.5(4.0)
Peak LVOT gradient(SD), mmHg	4.7(1.1)	6.2(2.2)	10.2(9.0)	77.9(193)
LVOT diameter(SD), cm	2.2(0.1)	2.2(0.2)	2.3(0.3)	2.2(0.3)
Wall motion score(SD)	8.8(8.9)	27.4(16.6)	18.2(14.4)	10.3(8.9)
Resting heart rate(SD), bpm	76.8(13.7)	74.2(11.6)	66.9(15.1)	70.7(10.5)
QTc interval(SD), ms	408(24)	398(32)	444(23)	424(37)

LVEF=left ventricular ejection fraction; GLS=global longitudinal strain; LVIDd = Left ventricular internal dimension at end-diastole; LVIDs = Left ventricular internal dimension at end-systole; LVEDV = left ventricular end-diastolic volume; LVEDVI = left ventricular end-diastolic volume index; RVEDV = right ventricular end-diastolic volume; RVEDVI = right ventricular end-diastolic volume index; IVSd=Interventricular septum thickness at end-diastole; LVPWd=Left ventricular posterior wall thickness at end-diastole; LAVI = left atrial volume index; SD = standard deviation;

Figure 1:

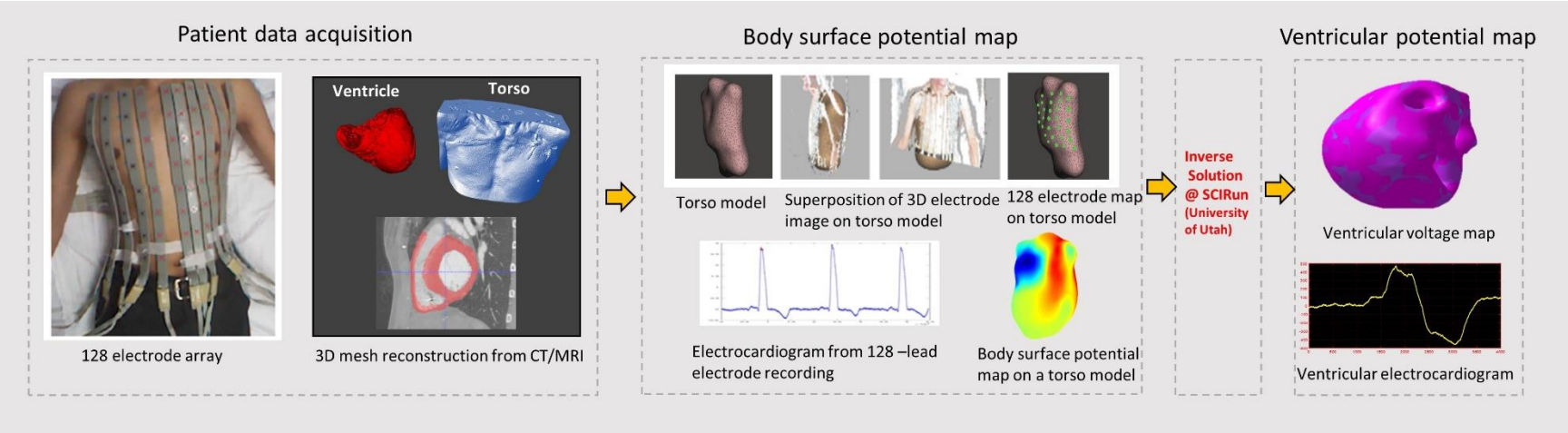
Patient data acquisition
Ventricle
Torso
128 electrode array
3D mesh reconstruction from CT/MRI
Body surface potential map
Torso model
Superposition of 3D electrode image on torso model
128 electrode map on torso model
Electrocardiogram from 128 –lead electrode recording
Body surface potential map on a torso model
Inverse Solution @ SCIRun (University of Utah)
Ventricular potential map
Ventricular voltage map
Ventricular electrocardiogram

Figure 2:

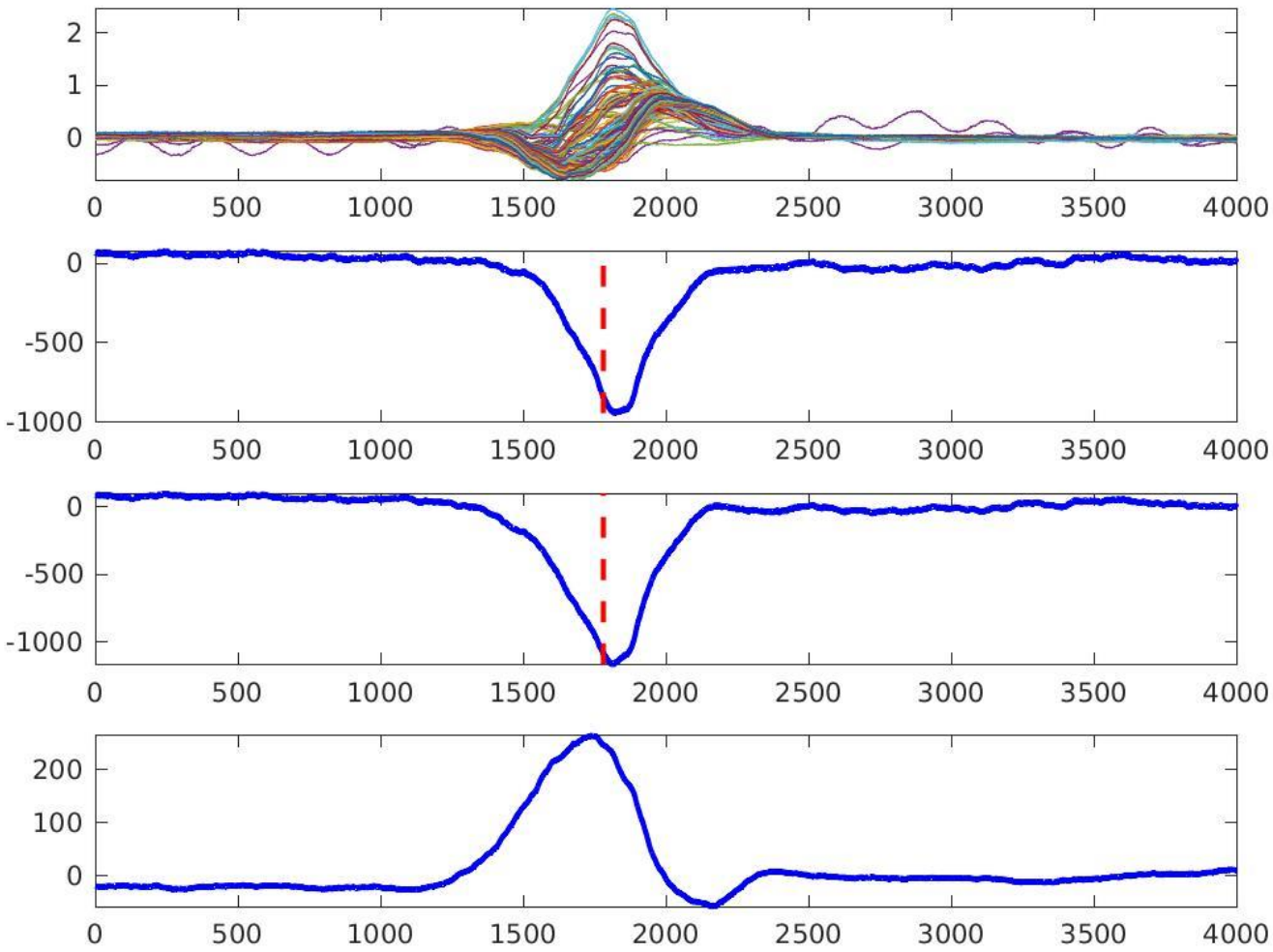
2
1
0
0
500
1000
1500
2000
2500
3000
3500
4000
0
-500
-1000
0
500
1000
1500
2000
2500
3000
3500
4000
0
-500
-1000
0
500
1000
1500
2000
2500
3000
3500
4000
200
100
0
0
500
1000
1500
2000
2500
3000
3500
4000

Figure 3:

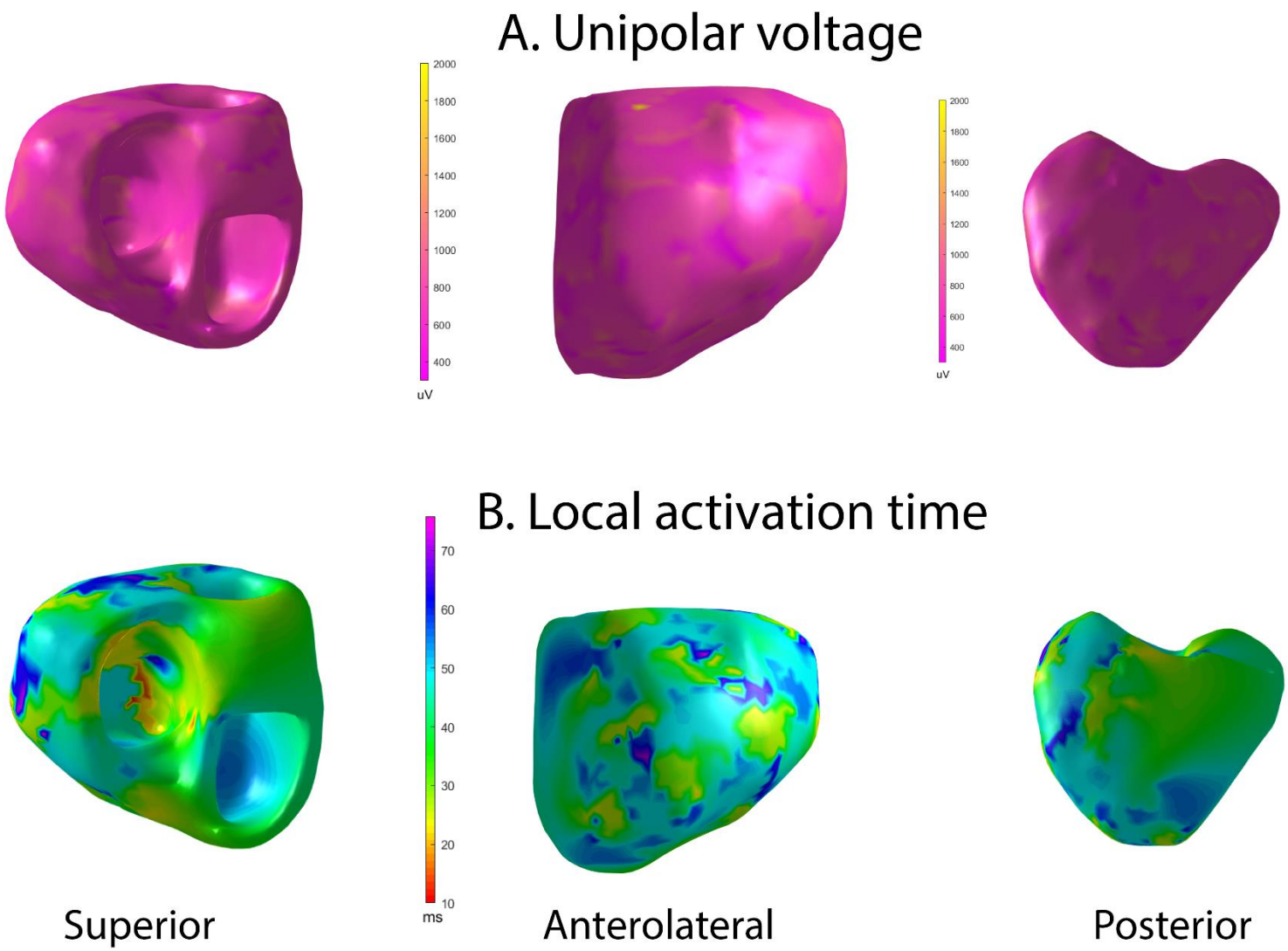
A. Unipolar voltage
2000
1800
1600
1400
1200
1000
800
600
400
uV
B. Local activation time
70
60
50
40
30
20
10
ms
Superior
Anterolateral
Posterior

Figure 4:

Mean (SD) unipolar voltage potentials (µV) in LV endocardial and epicardial, and RV endocardial septal regions

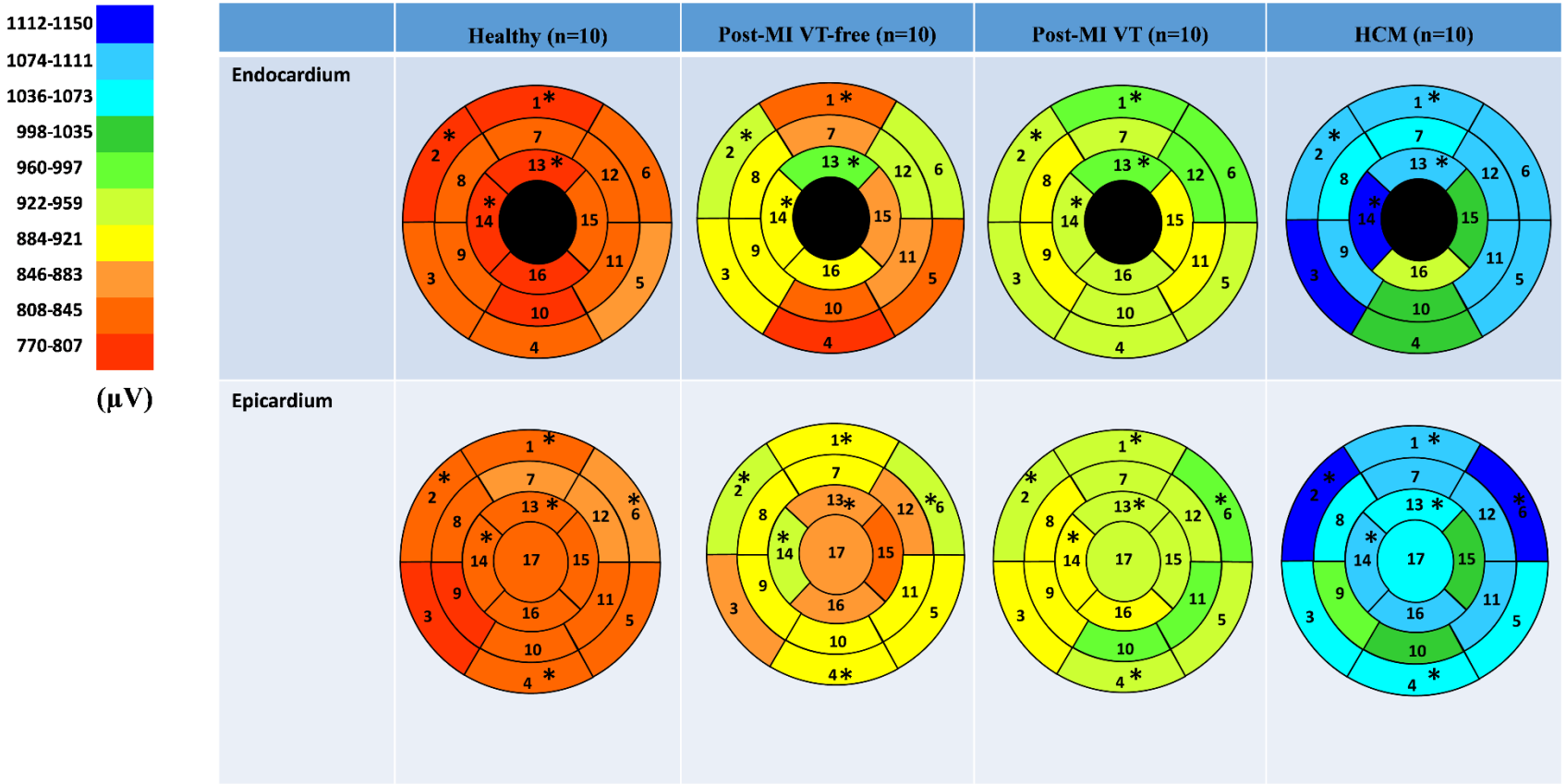

Figure 5:

Unipolar voltage dispersion within segments on endocardial and epicardial surface of the left ventricle

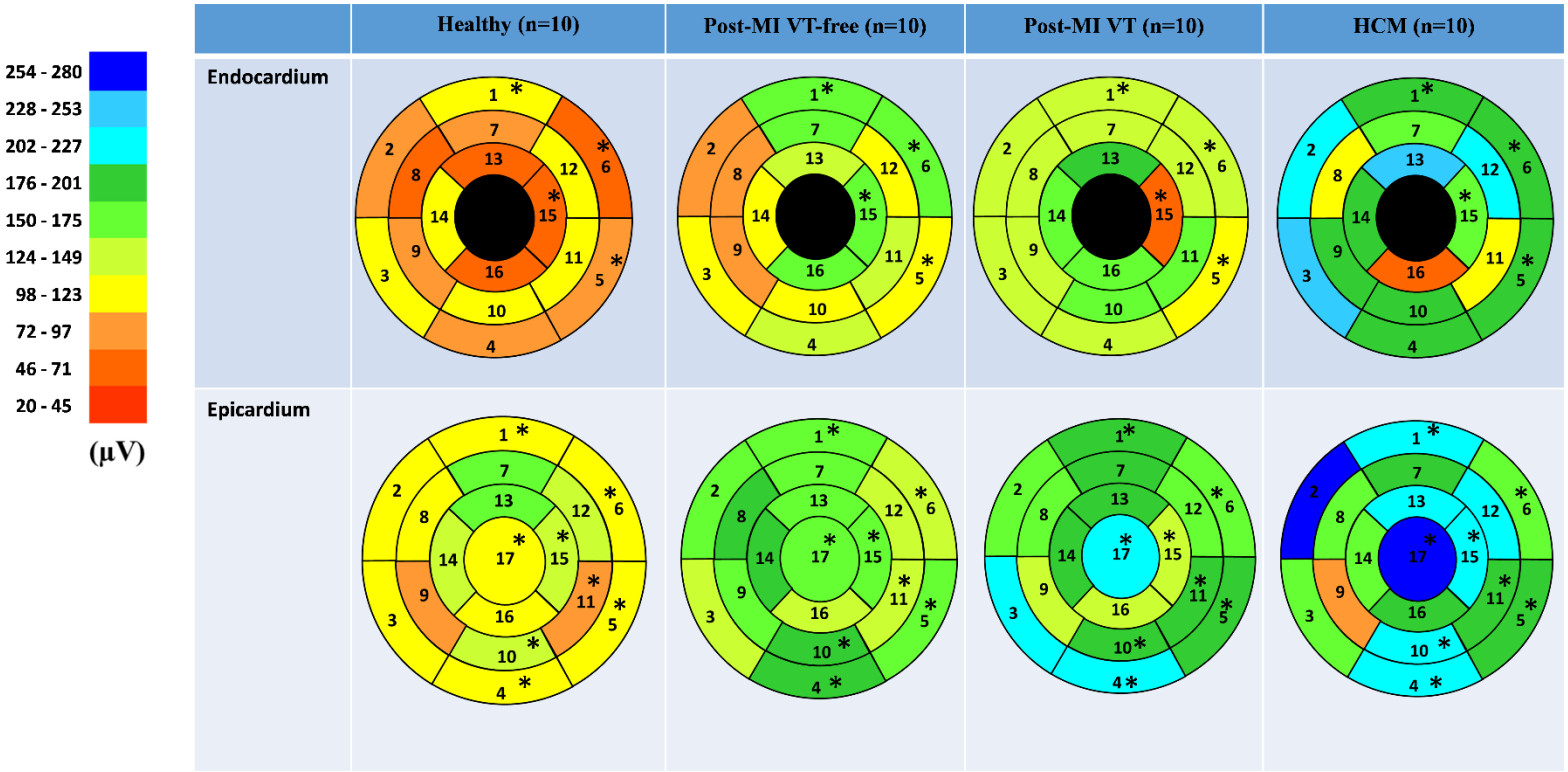

Figure 6:

Comparison of conduction velocity (cm/s) on endocardial and epicardial surface of the left ventricle

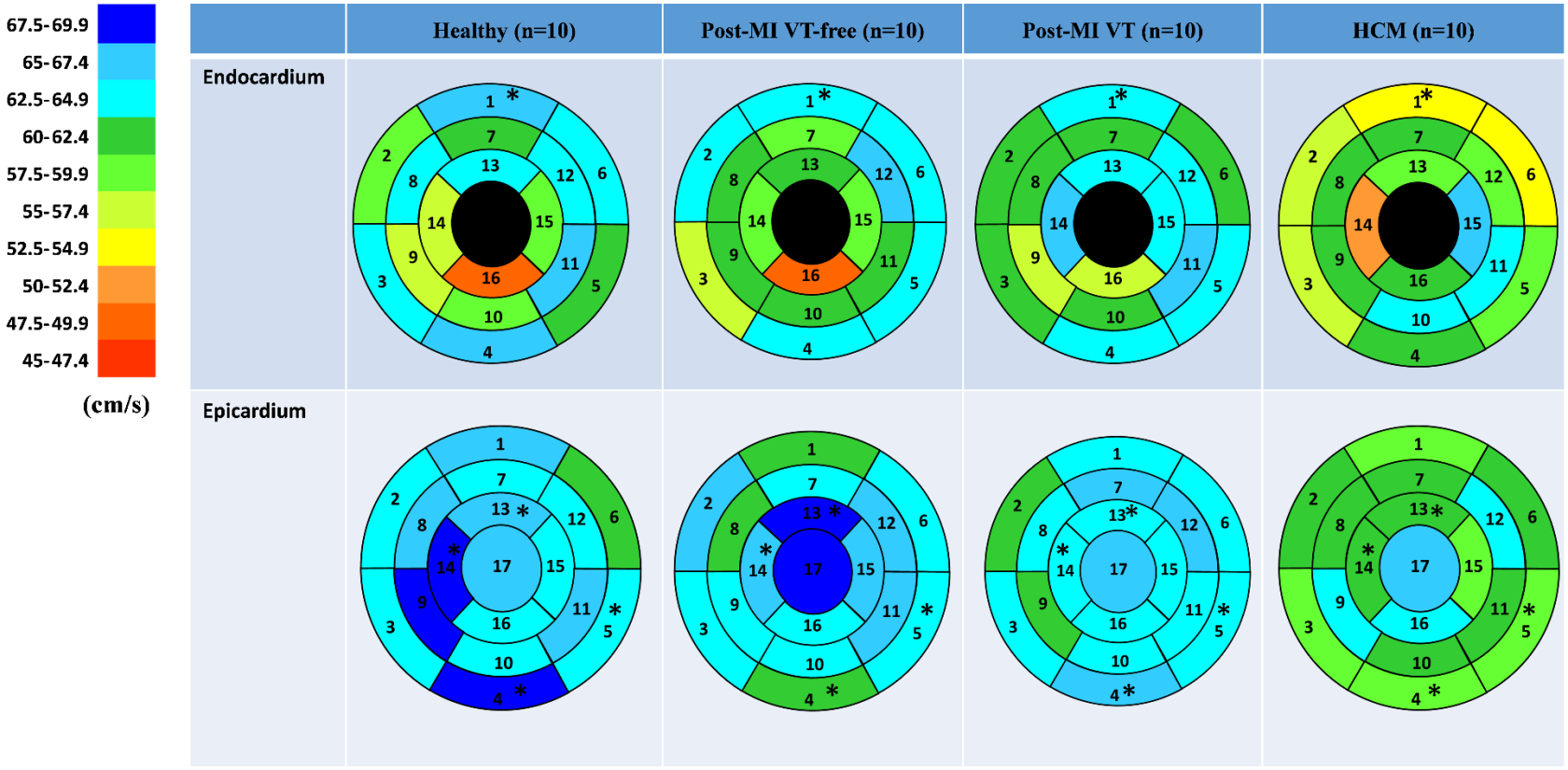

Suppl Table 1. Mean (SD) unipolar voltage potentials (µV) in LV endocardial and epicardial, and RV endocardial septal regions.

	Region	Healthy (n=10)	Post-MI VT-free (n=10)	Post-MI VT (n=10)	HCM (n=10)	P_{James}
Endocardial	Basal anterior	**802(108)**	**853(281)**	**982(230)**	**1086(241)**	**0.016**
	Basal anteroseptal	**812(128)**	**931(304)**	**954(166)**	**1085(266)**	**0.043**
	Basal inferoseptal	829(103)	901(359)	943(318)	1121(239)	**0.071**
	Basal inferior	823(106)	804(275)	942(241)	1037(276)	0.130
	Basal inferolateral	856(98)	835(291)	958(209)	1081(286)	0.125
	Basal anterolateral	**829(82)**	**949(337)**	**967(259)**	**1096(300)**	**0.023**
	Mid-anterior	838(114)	871(323)	945(187)	1045(214)	**0.090**
	Mid-anteroseptal	817(98)	903(291)	900(211)	1042(276)	0.136
	Mid-inferoseptal	839(107)	901(332)	916(224)	1087(290)	0.135
	Mid-inferior	793(83)	852(281)	952(262)	1008(251)	**0.071**
	Mid-inferolateral	836(98)	890(305)	926(260)	1111(297)	**0.086**
	Mid-anterolateral	837(94)	936(414)	984(238)	1110(244)	0.204
	Apical anterior	**809(111)**	**984(452)**	**969(154)**	**1094(314)**	**0.036**
	Apical septal	**810(133)**	**898(450)**	**941(205)**	**1122(229)**	**0.028**
	Apical Inferior	835(97)	863(282)	902(233)	1015(211)	0.198
	Apical lateral	791(143)	892(295)	964(181)	942(180)	0.133
Epicardial / RV endocardial	Basal anterior	**842(90)**	**898(358)**	**934(189)**	**1094(211)**	**0.023**
	RV_{endo} Basal anteroseptal	**827(157)**	**929(326)**	**961(174)**	**1120(217)**	**0.028**
	RV_{endo} Basal inferoseptal	808(133)	883(325)	904(234)	1073(302)	0.251
	Basal inferior	**838(99)**	**904(280)**	**964(228)**	**1053(177)**	**0.028**
	Basal inferolateral	847(113)	903(322)	936(177)	1069(205)	**0.064**
	Basal anterolateral	**855(131)**	**937(355)**	**996(166)**	**1125(218)**	**0.027**
	Mid-anterior	856(118)	901(307)	942(182)	1106(242)	**0.068**
	RV_{endo} Mid-anteroseptal	824(118)	912(415)	911(185)	1068(288)	0.201
	RV_{endo} Mid-inferoseptal	812(136)	893(349)	895(154)	975(231)	0.320
	Mid-inferior	838(88)	920(335)	966(229)	1002(211)	0.142
	Mid-inferolateral	**829(114)**	**904(341)**	**968(201)**	**1098(197)**	**0.013**
	Mid-anterolateral	856(107)	875(296)	941(165)	1076(215)	**0.069**
	Apical anterior	**825(102)**	**883(288)**	**950(195)**	**1075(241)**	**0.042**
	RV_{endo} Apical septal	**833(97)**	**937(365)**	**902(129)**	**1078(166)**	**0.008**
	Apical Inferior	829(102)	838(263)	933(166)	1024(188)	**0.068**
	Apical lateral	825(100)	884(360)	918(206)	1082(266)	**0.070**
	Apex	840(94)	888(320)	935(182)	1054(217)	**0.069**

Suppl Table 2. Unipolar voltage dispersion within segments on endocardial and epicardial surface of the left ventricle

	Region	Healthy (n=10)	Post-MI VT-free (n=10)	Post-MI VT (n=10)	HCM (n=10)	$P_{Kruskal\text{-}Wallis}$
Endocardial	Basal anterior	101(53-147)	161(102-214)	146(89-157)	178(162-276)	**0.017**
	Basal anteroseptal	73(42-132)	94(78-266)	148(64-227)	223(166-295)	0.053
	Basal inferoseptal	104(75-129)	123(84-199)	130(59-152)	230(155-314)	0.066
	Basal inferior	95(54-126)	126(79-152)	147(111-203)	184(130-267)	0.076
	Basal inferolateral	88(80-117)	114(89-153)	105(87-170)	177(124-252)	**0.031**
	Basal anterolateral	58(49-117)	153(128-195)	142(94-215)	201(136-224)	**0.049**
	Mid-anterior	82(73-105)	167(100-241)	127(80-229)	169(138-224)	0.113
	Mid-anteroseptal	50(36-59)	80(50-136)	127(48-171)	112(47-290)	0.345
	Mid-inferoseptal	87(54-117)	84(36-148)	125(66-204)	187(106-227)	0.277
	Mid-inferior	113(69)	111(79-285)	169(122-180)	183(72-196)	0.752
	Mid-inferolateral	110(48-176)	139(120-282)	158(112-197)	109(24-188)	0.368
	Mid-anterolateral	105(92-121)	112(83-196)	136(73-190)	219(48-335)	0.588
	Apical anterior	67(18-125)	141(76-170)	184(87-224)	248(102-306)	0.160
	Apical septal	107(106-127)	120(83-154)	170(113-233)	180(110-260)	0.222
	Apical Inferior	63(11-109)	151(97-229)	63(61-141)	155(106-199)	**0.035**
	Apical lateral	66(34-94)	160(102-202)	159(121-221)	63(23-163)	0.097
Epicardial / RV endocardial	Basal anterior	110(106-168)	158(109-236)	189(143-208)	215(161-281)	**0.041**
	RV Basal anteroseptal	112(105-150)	162(99-233)	152(91-201)	259(176-311)	0.109
	RV Basal inferoseptal	105(71-122)	135(90-229)	202(106-243)	172(117-319)	0.116
	Basal inferior	106(90-131)	179(146-323)	202(112-223)	207(130-311)	**0.019**
	Basal inferolateral	107(98-121)	151(131-185)	198(118-210)	185(167-290)	**0.004**
	Basal anterolateral	120(101-147)	145(135-161)	166(153-200)	172(140-268)	**0.025**
	Mid-anterior	150(128-163)	170(128-235)	195(166-234)	201(168-338)	0.060
	RV Mid-anteroseptal	106(49-134)	180(119-225)	150(112-191)	165(102-280)	0.187
	RV Mid-inferoseptal	90(69-123)	153(89-182)	136(92-167)	89(59-208)	0.338
	Mid-inferior	132(88-155)	178(116-260)	182(173-197)	217(151-277)	**0.040**
	Mid-inferolateral	79(75-134)	129(118-255)	190(132-228)	180(150-320)	**0.024**
	Mid-anterolateral	138(125-153)	145(99-144)	167(117-203)	217(156-248)	0.260
	Apical anterior	158(109-182)	163(124-275)	180(119-226)	220(175-244)	0.185
	RV Apical septal	129(95-149)	182(128-261)	194(161-219)	175(124-272)	0.070
	Apical Inferior	127(106-143)	150(128-179)	135(105-198)	222(152-261)	**0.047**
	Apical lateral	115(107-129)	126(105-207)	146(106-164)	182(156-341)	0.229
	Apex	118(100-129)	166(123-274)	206(130-229)	260(163-315)	**0.019**

Suppl Table 3. Comparison of mean conduction velocity (cm/s) on endocardial and epicardial surface of the left ventricle

	Region	Healthy (n=10)	Post-MI VT-free (n=10)	Post-MI VT (n=10)	HCM (n=10)	P_{James}
Endocardial surface	Basal anterior	66.1(5.4)	63.3(5.4)	64.0(8.0)	54.3(8.6)	**0.019**
	Basal anteroseptal	58.2(12.8)	63.8(6.5)	60.4(11.5)	56.3(11.5)	0.351
	Basal inferoseptal	64.0(6.5)	57.4(9.0)	61.1(7.0)	55.6(11.9)	0.301
	Basal inferior	67.2(8.0)	63.1(9.1)	63.6(8.1)	60.4(9.1)	0.424
	Basal inferolateral	60.3(8.3)	63.3(7.3)	63.1(7.0)	58.8(8.3)	0.552
	Basal anterolateral	63.1(6.3)	63.1(6.8)	61.0(14.0)	52.7(9.5)	0.054
	Mid-anterior	62.4(13.4)	58.9(11.5)	62.1(9.6)	60.0(6.1)	0.892
	Mid-anteroseptal	63.4(19.2)	61.9(8.7)	62.3(8.8)	61.7(17.4)	0.997
	Mid-inferoseptal	56.1(12.9)	62.2(12.4)	56.9(12.8)	60.2(12.8)	0.751
	Mid-inferior	59.2(9.5)	62.1(6.7)	61.2(16.0)	62.6(14.4)	0.898
	Mid-inferolateral	65.2(10.5)	62.2(6.4)	66.3(10.4)	63.4(14.6)	0.743
	Mid-anterolateral	63.0(6.5)	66.3(9.5)	63.2(11.2)	59.6(9.0)	0.516
	Apical anterior	63.4(22.5)	62.0(9.2)	64.4(8.5)	58.3(11.0)	0.713
	Apical septal	55.3(21.6)	59.6(10.9)	65.5(8.8)	50.2(14.5)	0.106
	Apical Inferior	58.2(16.7)	57.9(64.1)	64.1(8.6)	65.8(13.5)	0.335
	Apical lateral	48.4(24.6)	49.7(17.3)	56.4(16.9)	61.1(17.9)	0.681
Epicardial surface	Basal anterior	65.5(3.9)	62.4(3.9)	63.2(3.2)	63.2(3.2)	0.409
	RV Basal anteroseptal	64.4(5.9)	65.4(5.1)	60.7(5.5)	59.8(6.6)	0.119
	RV Basal inferoseptal	63.0(4.6)	64.7(4.0)	62.7(7.0)	62.1(7.7)	0.781
	Basal inferior	67.5(3.4)	61.5(3.4)	65.2(4.0)	59.1(5.6)	**0.001**
	Basal inferolateral	64.4(3.9)	62.7(6.0)	63.0(3.6)	58.1(6.1)	0.100
	Basal anterolateral	62.1(4.2)	63.9(5.3)	63.1(3.4)	57.5(4.1)	**0.014**
	Mid-anterior	63.8(6.9)	63.8(6.0)	65.7(4.3)	62.0(5.7)	0.478
	RV Mid-anteroseptal	65.0(8.1)	61.8(8.7)	64.0(11.6)	61.3(8.5)	0.845
	RV Mid-inferoseptal	68.2(12.3)	64.3(8.2)	60.9(13.6)	60.0(6.2)	0.374
	Mid-inferior	64.6(7.4)	64.8(7.4)	64.8(5.5)	64.3(5.1)	0.997
	Mid-inferolateral	66.9(3.1)	66.6(5.2)	63.9(7.2)	62.1(7.8)	0.294
	Mid-anterolateral	64.1(3.3)	65.4(4.5)	67.3(7.4)	62.1(3.6)	0.179
	Apical anterior	66.5(2.2)	69.2(2.5)	64.4(3.8)	64.6(6.2)	**0.013**
	RV Apical septal	68.9(2.5)	66.4(2.6)	62.7(5.7)	61.0(4.0)	**0.0002**
	Apical Inferior	63.2(6.1)	66.5(5.3)	64.0(10.5)	62.0(7.4)	0.471
	Apical lateral	64.9(6.4)	63.7(4.7)	63.5(12.1)	59.7(8.9)	0.573
	Apex	65.9(2.0)	68.7(3.3)	65.7(5.0)	64.9(3.9)	0.134

Suppl Table 4. Comparison of conduction velocity dispersion (cm/s) on endocardial and epicardial surface of the left ventricle

	Region	Healthy (n=10)	Post-MI VT-free (n=10)	Post-MI VT (n=10)	HCM (n=10)	$P_{Kruskal\text{-}Wallis}$
Endocardial surface	Basal anterior	21.2(20.6-22.1)	22.3(21.5-23.8)	22.2(21.1-22.8)	22.6(21.1-23.7)	0.372
	Basal anteroseptal	21.6(20.0-24.2)	23.0(21.7-23.7)	22.4(20.0-23.3)	23.6(20.5-23.7)	0.806
	Basal inferoseptal	21.7(21.4-23.0)	21.5(21.0-23.0)	21.2(21.1-21.8)	23.9(21.1-24.6)	0.307
	Basal inferior	20.9(19.9-21.5)	22.4(20.7-23.0)	21.8(20.7-23.0)	21.7(20.0-24.0)	0.520
	Basal inferolateral	22.0(20.0-23.1)	22.5(20.9-24.4)	22.5(22.2-23.6)	22.8(22.1-24.1)	0.610
	Basal anterolateral	23.1(21.1-23.4)	21.9(21.2-23.2)	21.2(19.7-22.5)	22.5(21.6-24.5)	0.517
	Mid-anterior	22.2(19.7-22.9)	21.9(20.9-23.2)	21.0(20.3-22.0)	21.9(21.6-23.7)	0.578
	Mid-anteroseptal	18.5(17.2-20.4)	22.7(21.4-23.5)	22.0(21.1-24.2)	20.6(17.9-23.4)	**0.015**
	Mid-inferoseptal	22.0(18.9-22.2)	21.0(19.7-22.2)	21.0(19.8-22.5)	21.6(20.0-23.6)	0.870
	Mid-inferior	23.2(20.5-24.7)	23.4(22.0-24.4)	20.7(15.3-23.6)	20.6(18.0-23.2)	0.313
	Mid-inferolateral	22.0(20.5-22.7)	22.6(21.5-23.5)	20.0(19.1-22.9)	21.0(19.2-21.6)	0.272
	Mid-anterolateral	22.5(21.0-23.0)	22.1(19.2-22.9)	21.2(19.7-22.8)	22.3(20.2-24.4)	0.600
	Apical anterior	18.7(18.1-20.4)	21.8(20.9-22.8)	21.9(20.5-23.4)	22.1(19.6-24.5)	0.641
	Apical septal	23.0(20.1-24.1)	21.1(19.2-22.6)	22.0(19.8-22.7)	19.1(14.8-22.4)	0.408
	Apical Inferior	19.2(17.1-21.3)	22.2(20.7-23.2)	20.7(18.2-22.0)	21.0(18.0-22.0)	0.072
	Apical lateral	17.5(10.5-18.8)	20.3(17.8-21.9)	20.5(16.0-22.3)	17.2(14.0-18.8)	0.151
Epicardial	Basal anterior	22.5(21.3-22.7)	22.8(21.9-23.9)	22.5(22.1-22.9)	22.5(22.3-22.8)	0.751
	RV Basal anteroseptal	22.6(22.0-23.8)	21.3(20.9-22.3)	22.6(21.2-23.5)	23.6(23.1-24.1)	**0.008**
	RV Basal inferoseptal	23.5(22.4-24.0)	22.7(21.6-23.2)	24.1(20.3-24.5)	21.8(20.2-22.7)	0.344
	Basal inferior	22.4(21.4-22.7)	23.0(22.0-23.9)	21.9(21.3-23.9)	22.9(21.8-23.8)	0.319
	Basal inferolateral	22.4(21.3-22.7)	22.3(21.7-23.0)	22.0(21.5-24.0)	24.0(22.8-24.0)	**0.064**
	Basal anterolateral	22.8(22.1-23.1)	23.3(22.6-23.3)	22.6(21.6-23.2)	22.6(22.1-24.2)	0.454
	Mid-anterior	22.7(21.8-23.2)	22.4(20.9-23.1)	21.6(21.2-22.3)	22.4(21.9-22.5)	0.319
	RV Mid-anteroseptal	21.7(20.4-22.3)	22.8(20.7-24.3)	21.6(17.9-24.7)	21.2(20.8-22.7)	0.761
	RV Mid-inferoseptal	19.7(17.0-22.1)	21.8(19.8-25.0)	19.9(18.4-21.5)	22.3(20.9-23.8)	0.128
	Mid-inferior	22.7(21.1-24.2)	22.2(21.0-23.1)	22.2(21.5-23.0)	21.3(20.6-22.6)	0.673
	Mid-inferolateral	21.9(21.5-23.3)	22.3(21.2-23.1)	21.7(20.3-22.7)	21.9(21.3-23.4)	0.754
	Mid-anterolateral	22.6(22.0-23.2)	23.0(21.4-24.0)	21.0(19.3-22.2)	23.0(22.3-23.5)	**0.037**
	Apical anterior	21.6(21.2-21.7)	20.9(20.6-21.1)	22.4(21.9-23.2)	21.9(21.3-24.0)	**0.013**
	RV Apical septal	21.8(21.2-22.1)	22.6(20.6-22.8)	22.1(21.4-22.5)	22.7(21.6-23.3)	0.212
	Apical Inferior	21.8(20.4-22.1)	21.4(20.5-23.5)	21.2(19.7-22.0)	22.7(22.0-23.9)	0.204
	Apical lateral	22.0(19.8-23.2)	23.9(20.6-24.7)	21.1(19.7-22.2)	22.1(19.8-23.6)	0.277
	Apex	22.2(21.5-22.7)	21.8(20.4-22.5)	21.7(21.0-22.6)	22.5(22.2-22.7)	0.228

Supplemental movies 1 and 2 show representative examples of unipolar voltage and ventricular activation maps in a healthy participant, during sinus rhythm activation.